Numerical simulation of impinging jet flows by modified MPS method

Zhenyuan Tang and Decheng Wan
State Key Laboratory of Ocean Engineering, School of Naval Architecture, Ocean and Civil Engineering, Collaborative Innovation Center for Advanced Ship and Deep-Sea Exploration, Shanghai Jiao Tong University, Shanghai, China

Received 4 January 2015
Revised 14 March 2015
Accepted 14 March 2015

Abstract

Purpose – The jet impingement usually accompanying large interface movement is studied by the in-house solver MLParticle-SJTU based on the modified moving particle semi-implicit (MPS) method, which can provide more accurate pressure fields and deformed interface shape. The comparisons of the pressure distribution and the shape of free surface between the presented numerical results and the analytical solution are investigated. The paper aims to discuss these issues.

Design/methodology/approach – To avoid the instability in traditional MPS, a modified MPS method is employed, which include mixed source term for Poisson pressure equation (PPE), kernel function without singularity, momentum conservative gradient model and highly precise free surface detection approach. Detailed analysis on improved schemes in the modified MPS is carried out. In particular, three kinds of source term in PPE are considered, including: particle number density (PND) method, mixed source term method and divergence-free method. Two typical kernel functions containing original kernel function with singularity and modified kernel function without singularity are analyzed. Three kinds of pressure gradient are considered: original pressure gradient (OPG), conservative pressure gradient (CPG) and modified pressure gradient (MPG). In addition, particle convergence is performed by running the simulation with various spatial resolutions. Finally, the comparison of the pressure fields by the modified MPS and by SPH is presented.

Findings – The modified MPS method can provide a reliable pressure distribution and the shape of the free surface compared to the analytical solution in a steady state after the water jet impinging on the wall. Specifically, mixed source term in PPE can give a reasonable profile of the shape of free surface and pressure distribution, while PND method adopted in the traditional MPS is not stable in simulation, and divergence-free method cannot produce rational pressure field near the wall. Two kernel functions show similar pressure field, however, the kernel function without singularity is preferred in this case to predict the profile of free surface and pressure on the wall. The shape of free surface by CPG and MPG is agreement with the analytical solution, while a great discrepancy can be observed by OPG. The pressure peak by MPG is closer to the analytical solution than that by CPG, while the pressure distribution on the right hand side of the pressure peak by latter is better match with the analytical solution than that by former. Besides, fine spatial resolution is necessary to achieve a good agreement with analytical results. In addition, the pressure field by the modified MPS is also quite similar to that by SPH, and this can further validate the reliable of current modified MPS.

The work is supported by National Natural Science Foundation of China (Grant Nos 51379125, 51490675, 11432009, 51411130131), National Key Basic Research Development Plan (973 Plan) Project of China (Grant No. 2013CB036103), Chang Jiang Scholars Program (T2014099), Program for Professor of Special Appointment (Eastern Scholar) at Shanghai Institutions of Higher Learning (Grant No. 2013022) and Center for HPC at Shanghai Jiao Tong University, to which the authors are most grateful.

Engineering Computations: International Journal for Computer-Aided Engineering and Software
Vol. 32 No. 4, 2015
pp. 1153-1171

0264-4401
DOI 10.1108/EC-01-2015-0002

Originality/value – The present modified MPS appears to be a stable and reliable tool to deal with the impinging jet flow problems involving large interface movement. Mixed source term in PPE is superior to PND adopted in the traditional MPS and divergence-free method. The kernel function without singularity is preferred to improve the computational accuracy in this case. CPG is a good choice to obtain the shape of free surface and the pressure distribution by jet impingement.

Keywords Free surface flow, Impinging jet flows, Kernel function, MPS (moving particle semi-implicit), Pressure Poisson equation (PPE)

Paper type Research paper

1. Introduction

Impinging jets are commonly encountered in a variety of industries such as pouring of liquids in containers, the atomization process of liquid impinging jets and fuel-coolant interaction in nuclear power plants. In these industry processes, impinging jet flows are usually accompanied by complex flow phenomena, such as large interface movement, the breakup of liquid sheet (Qiang, *et al.*, 2013) and air entrainment (Deshpande and Trujillo, 2013). Due to the complexity, analytical solution of such problem is quite difficult. The jet impinging on a flat plate was solved analytically by Michell (1890) based on strong hypothesis and the implicit expression for the pressure acting on the wall was given by Milne-Thomson (1962). Recently, computational fluid dynamics (CFD) has been an alternative and effective approach to study the impinging jet flow. Chihiro *et al.* (2008) used multi-interface advection and reconstruction solver and level-set method to simulate the atomization process of liquid sheet formed by impinging jets. Chen *et al.* (2013) proposed the atomization of impinging jet by combination of volume of fluid (VOF) and adaptive mesh refinement. Deshpande *et al.* (2012) investigated a circular water jet plunging into a quiescent pool at shallow inclination employing the interFoam solver of OpenFoam together with VOF.

All of the above numerical studies are based on grid system. Another alternative tool to study the jet impingement flows in CFD field is the meshless method (Reichl *et al.*, 1998; Antuono *et al.*, 2010). Moving particle semi-implicit (MPS) method is one such meshless Lagrangian particle method, first proposed by Koshizuka and Oka (1996), Koshizuka *et al.* (1998) to simulate the incompressible flow with large free surface deformation. The fluid is presented as a large amount of Lagrangian particles, whose physical properties evolve in time based on the governing equations. A main advantage of such method is the ability to deal with complex free surface flows without any special complex treatment, which is difficult to tackle in mesh-based method due to the numerical diffusion produced by the discretization of advection terms. By now, MPS method has been applied into numerous flow problems, such as dam breaking (Khayyer and Gotoh, 2012; Zhang and Wan, 2011a; Zhang *et al.*, 2011), breaking wave (Khayyer and Gotoh, 2008; Tang, *et al.*, 2014), sloshing (Zhang *et al.*, 2014; Zhang and Wan, 2014), ship-wave interaction (Shibata *et al.*, 2012; Zhang and Wan, 2011b) and green water (Zhang *et al.*, 2013). These works can further prove that MPS is a flexible numerical approach for violent free surface flows.

However, due to the strong pressure oscillation and the instability in traditional MPS, a massive effort has been made to suppress the pressure fluctuation and improve the computational stability and the computational accuracy by MPS practitioners. A high-order Laplacian model was derived and proposed by Khayyer and Gotoh (2010, 2012). A mixed source term for the Poisson pressure equation (PPE) was studied by Tanaka and Masunaga (2010) based on the original kernel function. The original

pressure gradient (OPG) model was first adopted by Koshizuka *et al.* (1998). Due to its non-conservation of system momentum, the method cannot obtain an acceptable pressure field. To overcome this, Tanaka and Masunaga (2010) suggested a conservative formula to improve the pressure field. Recently, Sriram and Ma (2008, 2012) proposed a new pressure gradient model using the simplified finite difference scheme (SFDI) in their particle method, where the irregular particle arrangement can be considered. Ataie-Ashtiani and Farhadi (2006) attempted to stabilize simulation by only changing weight functions, but the accuracy is not validated. Pan and Zhang (2008) discussed the effects of different kernel function to predict the impact pressure for sloshing problems by using area and time average method to treat the pressure oscillations. Zhang and Wan (2012) suggested a modified kernel function which can produce a good impact pressure combined with the mixed source term in PPE and an accuracy free surface detection. Unfortunately, the accuracy between these two kernel functions was not compared.

The main purpose of present work is to study the jet impingement by in-house particle solver MLParticle-SJTU based on modified MPS method, which includes four improved schemes: first, kernel function without singularity (Zhang and Wan, 2012); second, momentum conservative gradient model (Tanaka and Masunaga, 2010); third, mixed source term for PPE (Tanaka and Masunaga, 2010); and fourth, highly precise free surface detection approach (Zhang and Wan, 2012). The paper is organized in the following way. First, a brief introduction of the MPS method including governing equations and particle interaction models is presented. Next, a 2D water jet impinging on the wall, where both the shape of free surface and the pressure distribution along the wall are expressed analytically by Milne-Thomson (1962), is simulated to validate the modified MPS method. Detailed analysis on improved schemes including source term in PPE, kernel function, pressure gradient is carried out and the convergence is also validated by increasing the spatial resolution. In addition, the pressure distributions by SPH and by MPS are also compared to further validate the reliability of modified MPS.

2. Numerical scheme

2.1 Governing equations

In the MPS method, governing equations are the mass and momentum conservation equations. They can be expressed in Lagrangian form for incompressible fluid as:

$$\frac{1}{\rho}\frac{D\rho}{Dt} = -\nabla \cdot V = 0 \tag{1}$$

$$\frac{D\boldsymbol{V}}{Dt} = -\frac{1}{\rho}\nabla P + v\nabla^2 \boldsymbol{V} + \boldsymbol{g} \tag{2}$$

where the term D/Dt denotes the substantial derivative, ρ is the fluid density, P is the pressure, $\boldsymbol{V}$ is the velocity vector, $\boldsymbol{g}$ is gravitational acceleration vector, v is the kinematic viscosity, t is the time.

2.2 Particle interaction models

In MPS, the gradient operator is discretized as local weighted average of the gradient vectors between particles i and its neighboring particles j, it can be given as (Koshizuka *et al.*, 1998):

$$< \nabla P >_i = \frac{\dim}{n^0}\sum_{j \neq i}\frac{P_j - P_i'}{\left|\boldsymbol{r}_j - \boldsymbol{r}\right|^2}\left(\boldsymbol{r}_j - \boldsymbol{r}_i\right) \cdot W\left(\left|\boldsymbol{r}_j - \boldsymbol{r}_i\right|\right) \tag{3}$$

where subscript i, j represent the target particle and its neighbor particle, respectively, P presents the pressure and P_i' is the minimum pressure of neighboring particles around particle i, dim is the number of space dimensions, $\boldsymbol{r}$ is the position vector, n^0 is average initial particle number density (PND), $W(|\boldsymbol{r}_j-\boldsymbol{r}_i|)$ is kernel function. In the present work, an improved kernel function suggested by Zhang and Wan (2012) is adopted:

$$W(r)=\begin{cases}\frac{r_e}{0.85r+0.15r_e}-1 & 0\leqslant r<r_e\\ 0 & r_e\leqslant r\end{cases} \tag{4}$$

where $r=|\boldsymbol{r}_j-\boldsymbol{r}_i|$ is the distance between particle i and j, r_e is the radius of the support domain. This kernel function has a similar curve with the traditional kernel function (Koshizuka and Oka, 1996), but eliminates the singularity at the origin, which can avoid exaggerated repulse force between two neighboring particles with a very small distance. According to Koshizuka's numerical experiments (Koshizuka and Oka, 1996), it is not necessary to employ a common kernel size for particle interaction models. In the following simulations, the cut-off radius for PND (r_{e_Den}), gradient model (r_{e_Gra}), divergence model (r_{e_Div}) and Laplacian model (r_{e_Lap}) are employed as following: $r_{e\_Den}=2.1dp$, $r_{e\_Gra}=2.1dp$, $r_{e\_Div}=2.1dp$ and $r_{e\_Lap}=4.01dp$. dp is the initial distance between two neighboring particles.

Equation (3) cannot conserve the linear and angular momentum of the system, and a conservative form of gradient model is suggested by Tanaka and Masunaga (2010) as following:

$$<\nabla P>_i=\frac{\dim}{n^0}\sum_{j\neq i}\frac{P_j+P_i}{|\boldsymbol{r}_j-\boldsymbol{r}_i|^2}(\boldsymbol{r}_j-\boldsymbol{r}_i)\cdot W(|\boldsymbol{r}_j-\boldsymbol{r}_i|) \tag{5}$$

Similar to the gradient model, the divergence model for vector $\boldsymbol{V}$ can be formulated as (Tanaka and Masunaga, 2010; Shakibaeinia and Jin, 2012) :

$$<\nabla\cdot\boldsymbol{V}>_i=\frac{\dim}{n^0}\sum_{j\neq i}\frac{(\boldsymbol{V}_j-\boldsymbol{V}_i)\cdot(\boldsymbol{r}_j-\boldsymbol{r}_i)}{|\boldsymbol{r}_j-\boldsymbol{r}_i|^2}W(|\boldsymbol{r}_j-\boldsymbol{r}_i|) \tag{6}$$

The Laplacian operator is modeled by weighted average of the distribution of a quantity ϕ from particle i to its neighboring particles j, it can read as the following equations:

$$<\nabla^2\phi>_i=\frac{2\dim}{n^0\lambda}\sum_{j\neq i}(\phi_j-\phi_i)\cdot W(|\boldsymbol{r}_j-\boldsymbol{r}_i|) \tag{7}$$

$$\lambda=\frac{\sum_{j\neq i}W(|\boldsymbol{r}_j-\boldsymbol{r}_i|)\cdot|\boldsymbol{r}_j-\boldsymbol{r}_i|^2}{\sum_{j\neq i}W(|\boldsymbol{r}_j-\boldsymbol{r}_i|)} \tag{8}$$

where, the parameter λ is introduced to keep the variance increase equal to the analytical solution. In the following simulations, ∇^2P in the left hand side of the Poisson equation of pressure (Equation (15)) is discretized by Equation (7).

2.3 Detection of free surface particles

In the MPS method, the free surface dynamic condition is enforced by assigning zero pressure for surface particles and inaccuracy free surface particles may lead to unphysical pressure oscillations. Thus detecting surface particles is a significant point for free surface flow. By now, some approaches have been developed to detect the free surface particles. Koshizuka *et al.* (1998) recognized the surface particles according to the PND. Tanaka and Masunaga (2010) and Lee *et al.* (2011) judged the surface particle by using number of neighbor particles around the target particle. Khayyer *et al.* (2009) proposed a new criterion based on asymmetry of neighboring particles in which particles are judged as surface particles according to the summation of x-coordinate or y-coordinate of particle distance. In the present study, we employ a detection method (Zhang and Wan, 2012) which is also based on the asymmetry arrangement of neighboring particles, but uses different equations considering the weight between neighboring particles, aiming at describing the asymmetry more accurately, as follow:

$$\boldsymbol{F}_i = \frac{\dim}{n^0} \sum_{j \neq i} \frac{1}{|\boldsymbol{r}_i - \boldsymbol{r}_j|} (\boldsymbol{r}_i - \boldsymbol{r}_j) W(r_{ij}) \tag{9}$$

If the absolute of the function $\boldsymbol{F}$ at particle i is more than a threshold α, then particle i is considered as free surface particle, and this can be read as following:

$$|\boldsymbol{F}| > \alpha (\text{for free surface particles}) \tag{10}$$

where α is assigned to $0.9|\boldsymbol{F}|^0$, $|\boldsymbol{F}|^0$ is the initial value of $|\boldsymbol{F}|$ for surface particle (Figure 1).

3. Numerical simulations

In this section, a two-dimensional water jet impinging on a rigid plate is simulated to validate the particle interaction models. Figure 2 shows the set up of jet. The water jet of width $H = 0.4$ m impings on a solid wall with a velocity of $U = 1$ m/s without any physical viscosity. The angle between the axis of the water jet and solid wall is $\theta = \pi/6$. In all simulations, both the gravity and surface tension are ignored. The analytical solution has been presented by Milne-Thomson (1962), which can be expressed as Equations (11)-(14) as depicted in Figure 3. The angle of a generic point of the free surface is denoted by β, then the shape of free surface can be represented as following.

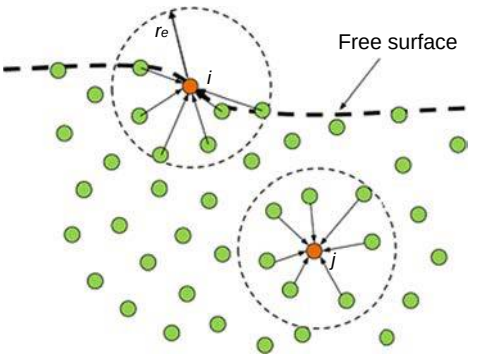

Figure 1.
A schematic view of the asymmetry arrangement of the neighboring particles

The shape of the left branch of the free surface ($\theta < \beta < \pi$):

$$\frac{x'}{H} = \frac{1}{\pi}\left\{\theta\sin\theta + \ln\left[\tan\left(\frac{\beta}{2}\right)\right] + \cos\theta\left[\ln\left(\frac{\sin\beta}{2}\right) - \ln\left(\sin\left(\frac{\theta+\beta}{2}\right)\sin\left(\frac{\beta-\theta}{2}\right)\right)\right]\right\} \tag{11}$$

$$\frac{y'}{H} = \frac{1}{\pi}\left\{\frac{\pi}{2}(1-\cos\theta) + \sin\theta\ln\left[\sin\left(\frac{\theta+\beta}{2}\right)\right] - \sin\theta\ln\left[\sin\left(\frac{\beta-\theta}{2}\right)\right]\right\} \tag{12}$$

The shape of the right branch of the free surface ($0 < \beta < \theta$):

$$\frac{x'}{H} = \frac{1}{\pi}\left\{(\theta-\pi)\sin\theta + \ln\left[\tan\left(\frac{\beta}{2}\right)\right] + \cos\theta\left[\ln\left(\frac{\sin\beta}{2}\right) - \ln\left(\sin\left(\frac{\theta+\beta}{2}\right)\sin\left(\frac{\theta-\beta}{2}\right)\right)\right]\right\} \tag{13}$$

$$\frac{y'}{H} = \frac{1}{\pi}\left\{\frac{\pi}{2}(1+\cos\theta) + \sin\theta\ln\left[\sin\left(\frac{\theta+\beta}{2}\right)\right] - \sin\theta\ln\left[\sin\left(\frac{\theta-\beta}{2}\right)\right]\right\} \tag{14}$$

3.1 Source term in PPE

In MPS, the projection method is adopted to ensure the incompressible condition. In each time step, there are two stages: first, temporal velocity of particles is calculated based on viscous force and gravitational force, and particles are moved according to the temporal velocity; second, pressure is implicitly calculated by solving a Poisson equation, then the velocity and position of particles are updated.

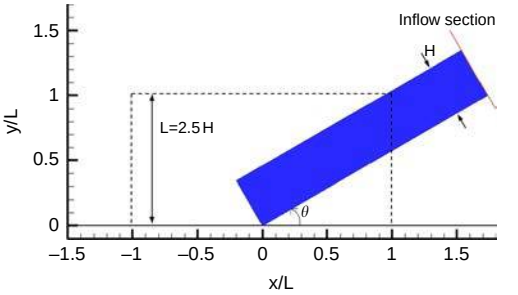

Figure 2.
Set up of the water jet impinging on a solid wall

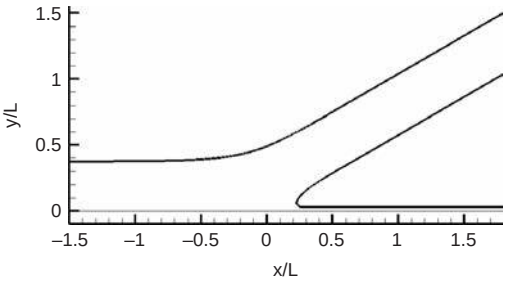

Figure 3.
The free surface solution for 2D jet acting on a solid wall

The Poisson equation of pressure in MPS method can be defined as following (Tanaka and Masunaga, 2010; Lee *et al.*, 2011):

$$< \nabla^2 P^{k+1} >_i = (1-\gamma)\frac{\rho}{\Delta t}\nabla \cdot \boldsymbol{V}_i^* - \gamma \frac{\rho}{\Delta t^2}\frac{n_i^k - n^0}{n^0} \tag{15}$$

where the superscript k and k+1 denote variables in kth and k+1th time level; γ is an artificial parameter with a value between 0 and 1, and it is also equivalent to the relative weighting of the deviation of PND from initial value and velocity divergence in the source term of PPE. If $\gamma = 1.0$, the right hand side of Equation (15) is only based on the variation of the temporal PND, and the formulation here becomes that first adopted in the traditional MPS (hereinafter denoted as PND method). In the numerical experiment, the PND method usually provides an exaggerated pressure oscillation due to the unsmoothed PND field. If $0 < \gamma < 1$, the source term of PPE is represented by the combination of the deviation of the temporal PND and velocity divergence, which is developed by Tanaka and Masunaga (2010). Here, this condition is called mixed source term method. Because the divergence of the velocity field is comparatively smoother than PND field even though the particles arrangement disorder, the Divergence-Free condition can enhance the smooth of the source term and further improve the pressure distribution. Generally, the smaller γ is, the smoother the pressure is. However, too small γ cannot ensure the volume conservation. Based on a large amount of numerical experiments carried out by Lee *et al.* (2011), the range of $0.01 \leqslant \gamma \leqslant 0.05$ seems to give a reasonable pressure distribution and keep the fluid volume conservation. If $\gamma = 1.0$, the source term of PPE is only controlled by the divergence of the velocity, which is commonly employed in the mesh-based method. This method is referred as Divergence-Free method. In the following, three simulations are carried out by PND method, mixed source term method and Divergence-Free method, respectively. The computational parameters are summarized in Table I as following, where d is the initial particle space.

In this section, Case A1 fails to predict the evolution of the water jet impinging on the wall. In MPS, a fraction step algorithm is employed, and the particles move to temporal positions first under the action of gravity and viscous force. When the gravity and viscous force are not considered, the simulation in Case A1 may lead to instability due to the large pressure fluctuations caused by unsmoothed PND field. Nevertheless, the simulations in Cases A2 and A3 are stable where the divergence of velocity is included in the source term of PPE. This can prove that the divergence of the velocity may play an important role in the computation stability. In addition, pressure fields provided by Cases A2 and A3 are shown in Figure 4, where the red solid line represents the shape of free surface by analytical solution. There are some great discrepancies between the pressure field by Case A2 and that by A3. The contour of the pressure by A3 is much clearer than that by A2, but the maximum pressure by A3 is about a half of that by A2. The pressure field by A3 is obviously unphysical because the position of maximum pressure happens in the corner of the right branch of the free surface but not

Table I. The main computational parameters for three kinds of PPE source terms

Case	Particle space (H/d)	Time step (s)	γ in PPE	Description
A1	80	2.0×10^{-4}	$\gamma = 1.0$	PND method
A2			$\gamma = 0.01$	Mixed source term method
A3			$\gamma = 0.0$	Divergence-free method

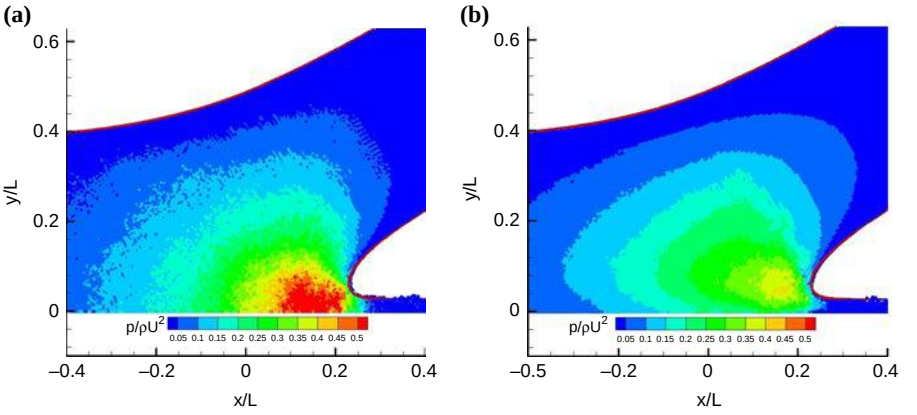

Figure 4.
The pressure field predicted by different source term ($H/d = 80$)

Notes: (a) Mixed source term method; (b) divergence free method

on the wall, while A2 provides a relatively reasonable pressure field. The reason maybe that the fluid volume can hardly keep conservation in the Divergence-Free method and unphysical particle clustering happens. This phenomenon can be proved by the PND field in Figure 5(b) where the fluid particles are clustering together near the solid wall. For a long time simulation, the particle clustering may lead to inaccuracy divergence of the velocity and effect the coefficient matrix in the left hand side of the PPE. Furthermore, this can cause an unphysical pressure field. In the view of numerical simulations, a reasonable pressure field should be achieved even though the irregular particle distribution. In fact, the irregular particle distribution may lead to low accuracy of the Laplacian model. The Laplacian model is only rough approximation, and it can keep accuracy only when the neighbor particles are symmetrical about the target particle. High accurate Laplacian model should be investigated further.

Figure 6 shows the pressure distribution along the plate by Cases A2 and A3. Although the overall tendencies in these cases are similar, Case A3 is not able to give an

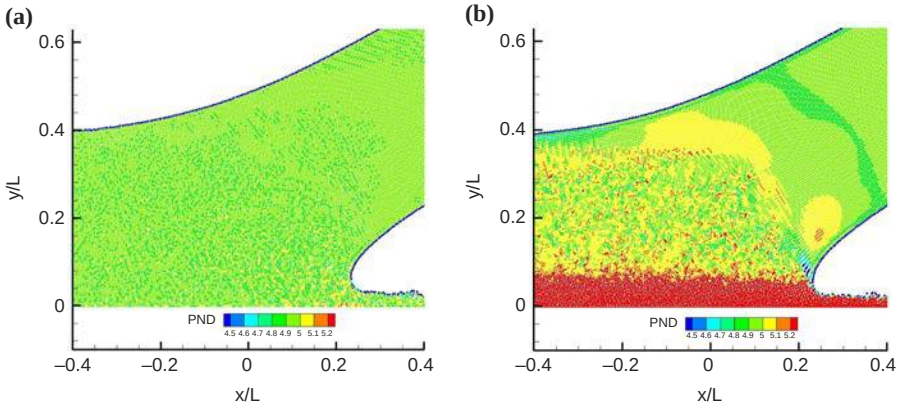

Figure 5.
The PND field predicted by different source term ($H/d = 80$)

Notes: (a) Mixed source term method; (b) divergence free method

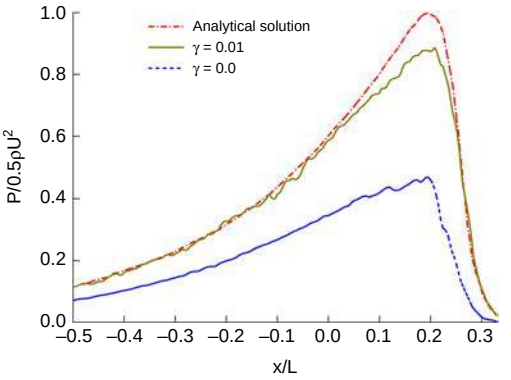

Figure 6.
The pressure distribution on the solid wall

acceptable pressure distribution while the pressure distribution by Case A2 shows a good match with the analytical solution except the value of the pressure peak. In Section 3.4, it can be proved that the discrepancy between the maximum of the pressure on the wall by A2 and the analytical solution can decrease when increasing the space resolution. On the other hand, the maximum pressure acting on the wall by Case A3 is nearly a half of that by Case A2. Specially note that the simulation is convergent when we focus on the shape of free surface, but the pressure field is still oscillating. Nevertheless, the average pressure on the time level is stable and the pressure distribution along the solid wall is the average value in one second. In the following sections, this treatment is also employed.

3.2 Effects of kernel functions

In MPS particle method, governing equations are transformed into the equations of particle interactions. These particle interactions are based on the kernel function. A reasonable kernel function can not only improve the computational accuracy, but also enhance the computational stability. In traditional MPS method, the kernel function is commonly adopted as following (Koshizuka *et al.*, 1998):

$$W(r) = \begin{cases} \frac{r_e}{r} - 1 & 0 < r < r_e \\ 0 & r_e \leqslant r \end{cases} \tag{16}$$

A main drawback of this kernel function is that it is mathematically singular at the origin $r = 0$. This can avoid particle clustering when two neighboring particles are too close. However, this may produce a large repulsive force between two neighboring particles with a small distance since it is infinite at $r = 0$. For violent flows, the singularity may lead to unphysical pressure. To overcome this, a modified kernel function is suggested by Zhang and Wan (2012), which can be expressed as Equation (4). Because the modified kernel function has a similar curve shape with Koshizuka's kernel function as seen in Figure 7, the cut-off radius of particle interaction domain, $r_e = 2.1dp$ or $4.0ldp$, are still valid for the modified kernel function. In this section, the effects of these two kernel functions are discussed and tested, and the corresponding computational parameters are shown in Table II.

The pressure fields predicted by Cases B1 and B2 are shown in Figure 8. The discrepancy between the shape of free surface by B1 and the analytical solution in the

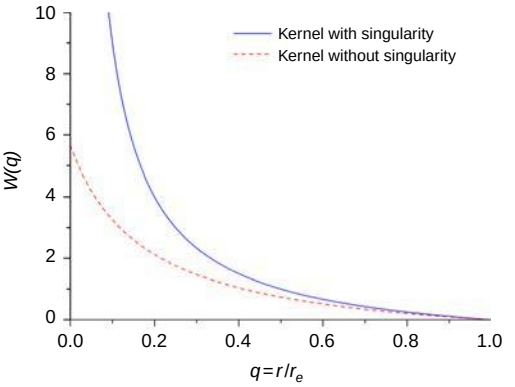

Figure 7.
Comparison between two kernel functions

Table II.
The computational parameters for two kernel functions

Case	Particle space (H/d)	Time step (s)	PPE source term	Kernel function
B1	80	2.0×10^{-4}	$\gamma = 0.01$	Singularity kernel function
B2				Non-singularity kernel function

corner of the right branch free surface can be observed obviously, while the shape of free surface by Case B2 shows a good match. In addition, the contours of pressure field are quite similar, and the positions of the maximum pressure are also very close. As shown in Figure 9, the pressure distributions along the plate in these two cases are similar to the theoretical solution except that the maximum pressures are smaller than analytical solution. However, this discrepancy can decrease when increasing the spatial resolution. Finally, the profile of pressure distribution on the right hand side of the pressure peak by Case B1 is slightly larger than that by Case B2 together with the analytical solution. This means that the force fields by these two kernel functions are slightly different. In general, the kernel function without singularity is preferred in this case to produce the profile of free surface and pressure on the wall.

3.3 Effects of the pressure gradient

In MPS, the pressure gradient needs to be calculated to update the velocity and positon of particles. Here, three kinds of pressure gradient models are considered. The main computational parameters for these cases are summarized as Table III. Considering the computational stability, only the modified pressure gradient (MPG) using the SFDI by Sriram and Ma (2012) is adopted in Case C3, where the pressure gradient can be expressed as following:

$$\langle P_x \rangle_i = \frac{C_{i,1} - a_{i,12} C_{i,2}}{1 - a_{i,12} a_{i,21}} \tag{17}$$

$$\langle P_y \rangle_i = \frac{C_{i,2} - a_{i,21} C_{i,1}}{1 - a_{i,12} a_{i,21}} \tag{18}$$

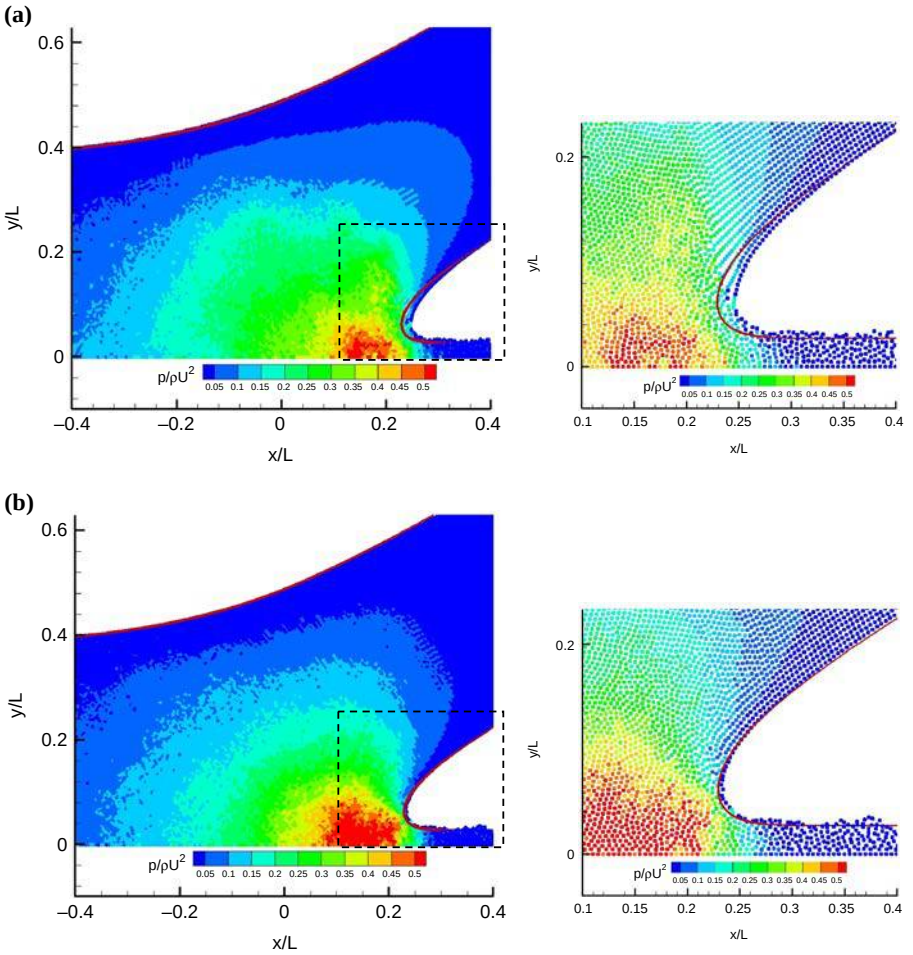

Notes: (a) Singularity kernel function; (b) nonsingularity kernel function

Figure 8.
The pressure field by different kernel functions

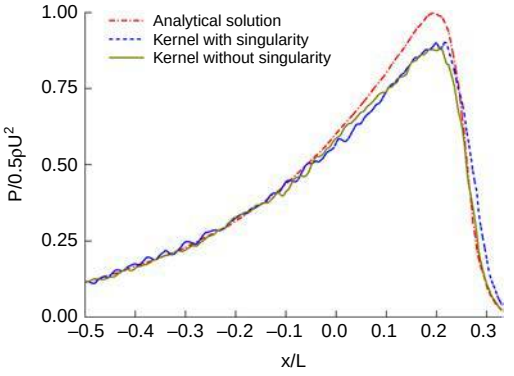

Figure 9.
The profiles of pressure acting on the solid plate by different kernel functions

where:

$$a_{i,mk} = \frac{1}{n_{i,m}} \sum_{j \neq i} \frac{(\boldsymbol{r}_{j,m} - \boldsymbol{r}_{i,m})(\boldsymbol{r}_{j,k} - \boldsymbol{r}_{i,k})}{|\boldsymbol{r}_j - \boldsymbol{r}_i|^2} W(\boldsymbol{r}_j - \boldsymbol{r}_i) \tag{19}$$

$$C_{i,m} = \frac{1}{n_{i,m}} \sum_{j \neq i} (P_j - P_i') \frac{(\boldsymbol{r}_{j,m} - \boldsymbol{r}_{i,m})}{|\boldsymbol{r}_j - \boldsymbol{r}_i|^2} W(\boldsymbol{r}_j - \boldsymbol{r}_i) \tag{20}$$

$$n_{i,mk} = \sum_{j \neq i} \frac{(\boldsymbol{r}_{j,m} - \boldsymbol{r}_{i,m})^2}{|\boldsymbol{r}_j - \boldsymbol{r}_i|^2} W(\boldsymbol{r}_j - \boldsymbol{r}_i) \tag{21}$$

where $W(\boldsymbol{r}_j - \boldsymbol{r}_i)$ is a weight function, P_i' is the minimum pressure of neighboring particles around the particle *i,* and subscript *m, k* is *x* and *y* coordinates, respectively.

Figure 10 illustrates the particle arrangement together with the distribution of pressure for OPG, conservative pressure gradient (CPG) and MPG. Both the CPG and MPG give an acceptable shapes of free surface, while the deviation of the shape of the right branch free surface by OPG from the analytical solution is evident and the change of curvature by OPG is smaller than the analytical one together with that by CPG and MPG. This means that OPG can ensure the computational stability but not the accuracy shape of free surface in this case. Furthermore, the contours of the pressure field among OPG, CPG and MPG are similar to each other in general. All the maximum pressures in these cases appear near the corner of the right branch free surface.

In Figure 11, the pressures distribution acting on the solid wall by OPG, CPG and MPG are depicted together with the analytical solution by Milne-Thomson (1962). Although the maximum pressure by OPG is larger than that by CPG and much closer to the analytical solution, the position of the pressure peak by the former shifts right compared with that by the latter together with MPG and analytical solution. On the other hand, the pressure peak by MPG is also larger than that by CPG, but with the same pressure peak position with CPG. This discrepancy between the CPG and MPG can prove that the pressure field by MPG is superior to that by CPG. The reason perhaps lies in the disorder particle distribution. In CPG, the pressure gradient model is deduced with the assumption that the neighboring particles are arranged uniformly around particle *i*. In fact, particles are distributed irregularly during the simulation, which may lead to the low accuracy of the pressure gradient in Case C2. On the contrary, the MPG can lead to a high-order accuracy even through the irregular particle arrangement. Therefore, MPG can provide a more agreeable pressure distribution than

Table III.
The computational parameters for different pressure gradient models

Case	Particle space (H/d)	Time step (s)	PPE source term	Pressure gradient	Description
C1	80	2.0×10^{-4}	$\gamma = 0.01$	Equation (3)	Original pressure gradient (OPG)
C2				Equation (5)	Conservative pressure gradient (CPG)
C3				Equations (17) and (18)	Modified pressure gradient (MPG)

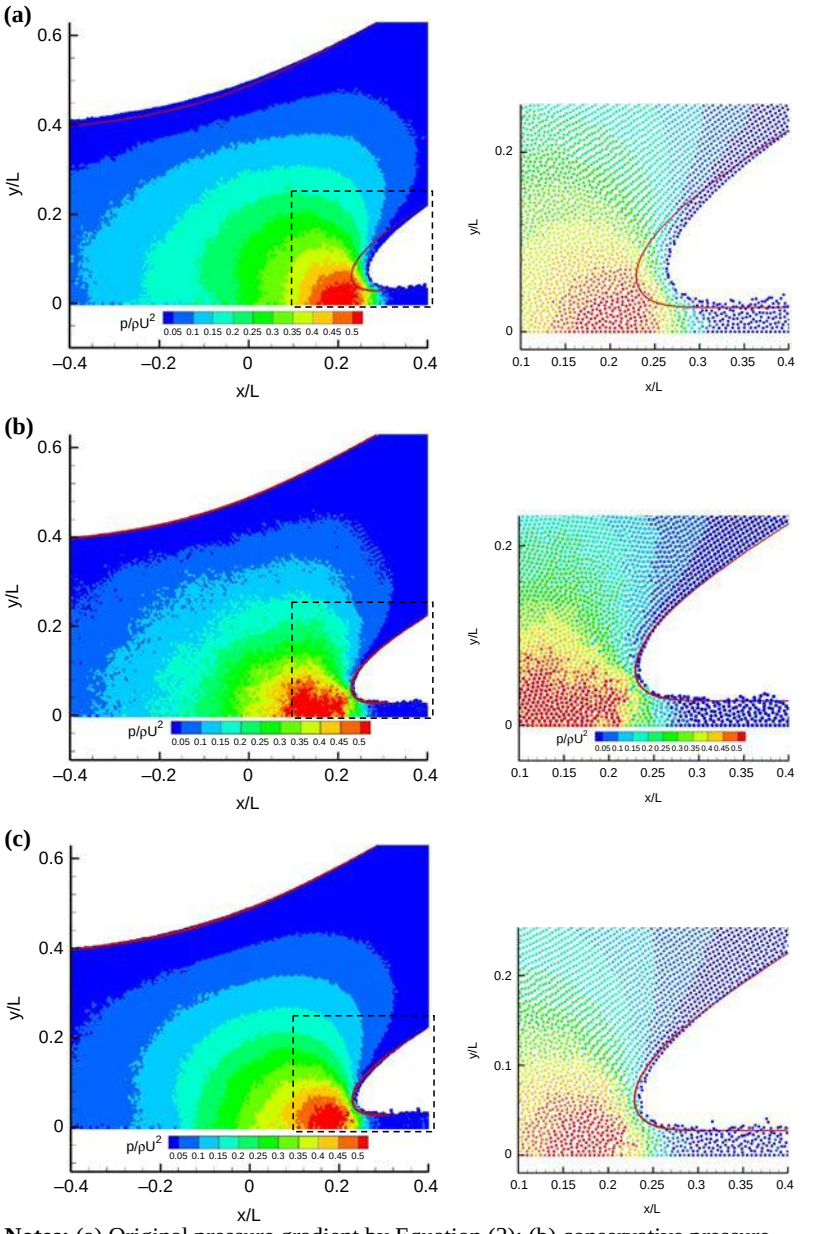

Notes: (a) Original pressure gradient by Equation (3); (b) conservative pressure gradient by Equation (5); (c) modified pressure gradient by Equations (17) and (18)

Figure 10.
The pressure field by different pressure gradient

CPG. Nevertheless, the pressure on the right hand side of the pressure peak position by CPG is agreeable with the analytical solution, but is overestimated by MPG.

These results show that OPG cannot provide an acceptable shape of free surface and the pressure distribution acting on the wall, while both CPG and

MPG can obtain accurate shape of free surface and agreeable position of the maximum pressure. The value of pressure peak by MPG is larger than that by CPG and much closer to the analytical solution, but the pressure distribution by CPG is much closer to the analytical solution on the right hand side of the pressure peak position.

3.4 Effects of space resolution

As to the mesh-based method, spatial resolution plays an important role on the computation accuracy for meshless method. In this section, effects of particle spaces on the accuracy of the shape of free surface and the pressure distribution acting on the solid plate are discussed. Here, three different simulations are carried out changing the spatial resolutions H/d = 40, 80, 160, together with mixed source term and kernel function without singularity. The computational conditions are listed in Table IV.

The pressure fields for different spatial resolutions are shown in Figure 12. All these cases can give an acceptable shape of free surface compared with the analytical solution represented by Milne-Thomson (1962). Figure 13 shows the comparison of the pressure distribution acting on the solid wall evaluated with different spatial resolutions. The tendencies of the pressure distribution and the position of the pressure peak in these cases are similar to the analytical solution in general. Although the maximum pressures in Cases D1 and D2 are less than the analytical one, the discrepancy between the numerical pressure peak and the analytical one decreases when increasing the spatial resolution.

Figure 14 illustrates the steady pressure field obtained by MPS, Riemann-SPH, δ-SPH and explicit-ISPH (Touzé *et al.*, 2012). As described in the literature, δ-SPH seems to present the best compromise of the pressure field and the shape of free surface. Here,

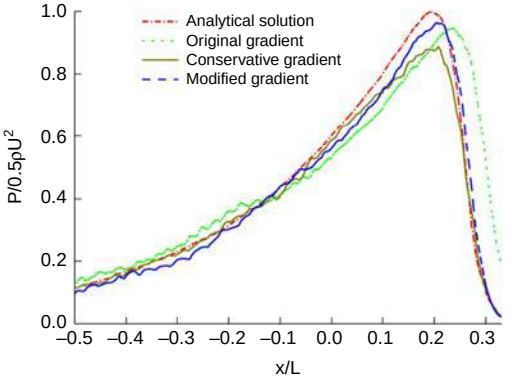

Figure 11.
The profiles of pressure acting on the solid plate by different pressure gradient models

Table IV.
The computation parameters for different particle spaces

Case	Particle space (H/d)	Time step (s)	Kernel function	PPE source term
D1	40	4.00×10^{-4}	Non-singularity kernel function	Mixed source term $\gamma = 0.01$
D2	80	2.00×10^{-4}		
D3	160	1.00×10^{-4}		

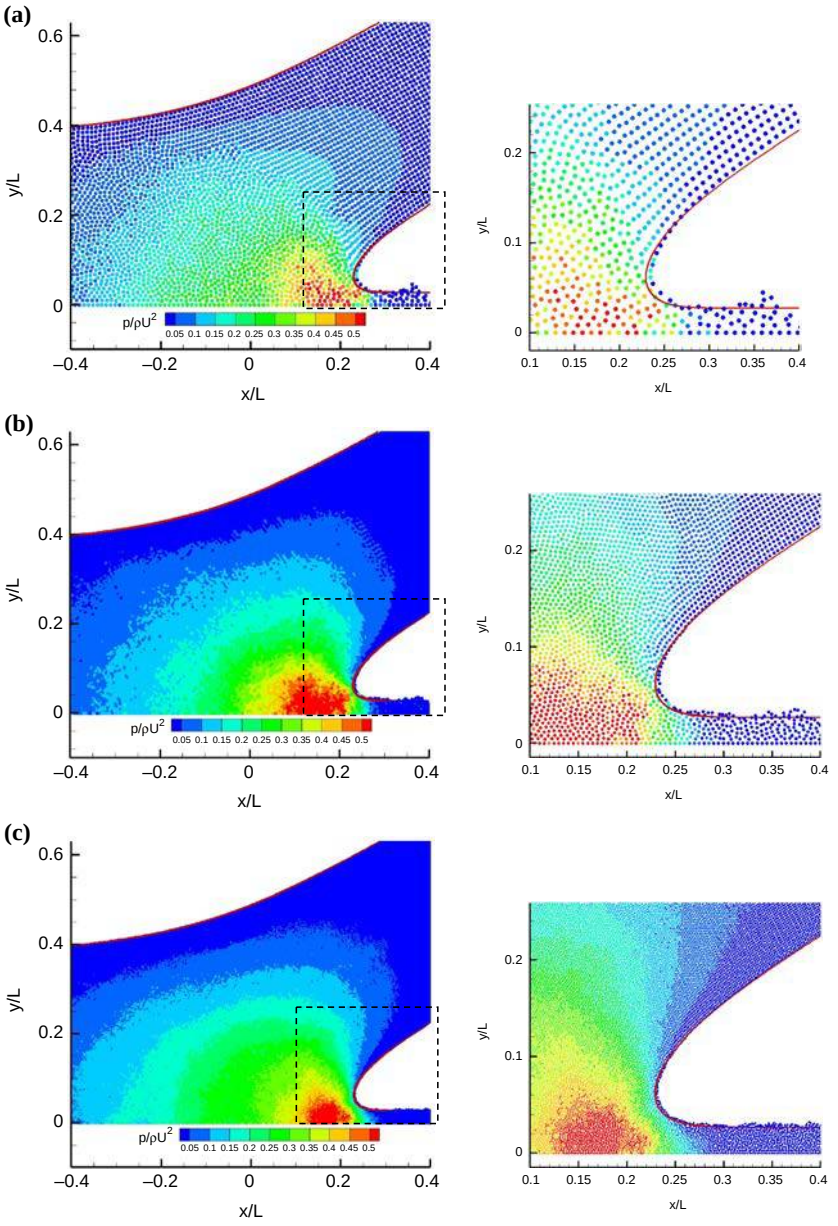

Notes: (a) $H/d = 40$; (b) $H/d = 80$; (c) $H/d = 160$

Figure 12.
The pressure field by different spatial resolution

the pressure field and the shape of free surface by the modified MPS are quite similar to that by δ-SPH. Unlike the δ-SPH, the artificial viscous and artificial density diffusion are not necessary for numerical stabilization. This can further prove the reliability of MPS method adopted here.

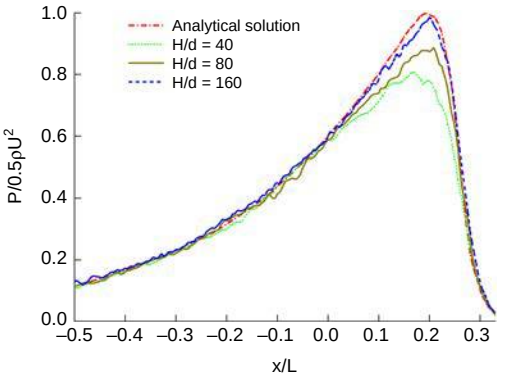

Figure 13.
The profile of pressure acting on the solid plate by different spatial resolution

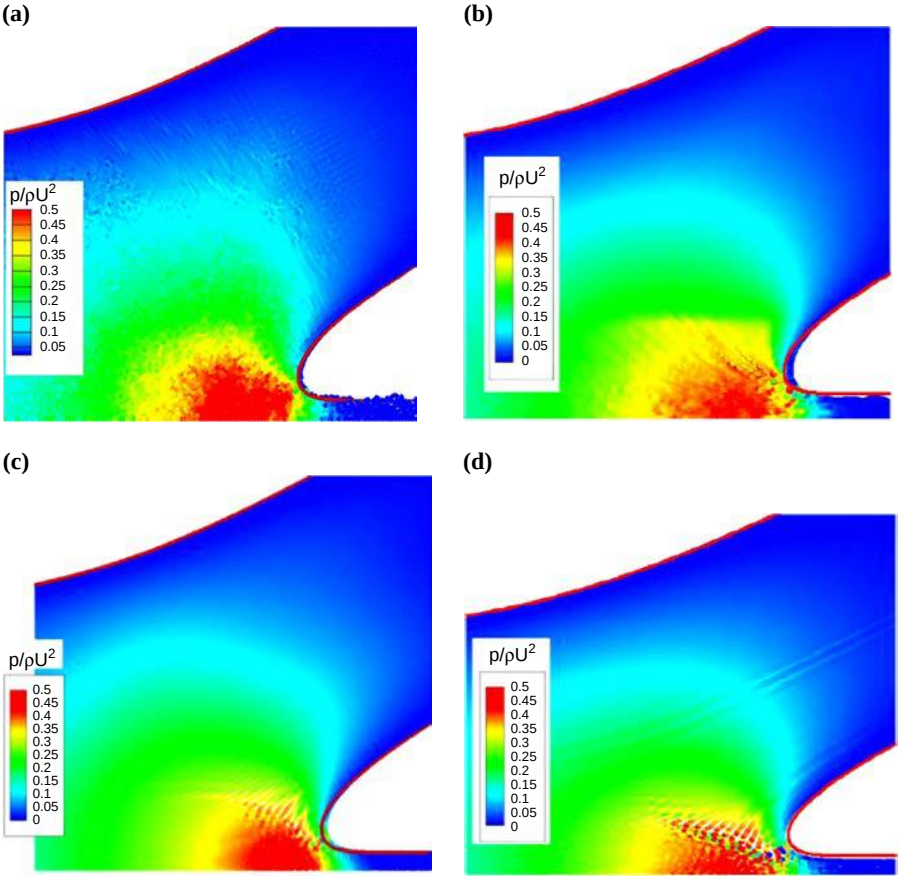

Figure 14.
Comparison between MPS and SPH (H/d = 80)

Notes: (a) MPS; (b) riemann-SPH; (c) δ-SPH; (d) explicit-ISPH

4. Conclusions

In this paper, a jet impingement having complex interface movement is simulated by our in-house particle solver MLParticle-SJTU based on the modified MPS method, including: mixed source term for PPE, kernel function without singularity, momentum conservative gradient model and highly precise free surface detection approach. Detailed analysis on the effect of source term in PPE, kernel function and pressure gradient in modified MPS is presented. First, three kinds of PPE source terms are considered: PND method, mixed source term method and divergence-free method. Results show that mixed source term method is superior since it agrees better with analytical results in terms of free surface profile and pressure field, while PND method is not stable in simulation, and divergence-free method cannot produce rational pressure field near the wall. In addition, effects of kernel functions are analyzed using two typical kernel functions: original kernel function with singularity and modified kernel function without singularity. These two kernel functions show similar pressure fields. However, the kernel function without singularity is preferred in this case to predict the profile of free surface and pressure distribution on the wall. Third, three kinds of pressure gradient are discussed: OPG, CPG and MPG. Both the CPG and MPG are superior to OPG since OPG cannot provide an acceptable shape of free surface and the pressure distribution acting on the wall. However, the value of pressure peak by MPG is larger than that by CPG and much closer to the analytical solution, but the pressure distribution on the wall by CPG is much closer to the analytical solution on the right hand side of the pressure peak position. Finally, particle convergence is validated by running the simulation with various spatial resolutions. Results also show that it is necessary to use fine spatial resolution to achieve a good agreement with analytical results. Furthermore, comparison between the pressure distributions by SPH and by MPS shows that the modified MPS can provide the similar shape of free surface as Riemann-SPH, δ-SPH and explicit-ISPH.

The present work has shown the capacity of the modified MPS method in studying the impinging jet flow with large interface movement. This method can be applied to a lot of industrial processes such as pouring of liquids in containers, the atomization process of two liquid impinging jets. In addition, based on the numerical experiments, increasing the spatial resolution can improve the computational accuracy, but lead to the computational cost increasing sharply. The overlapping particle technique can be introduced to improve the computational efficiency with refining the flow field in the concerned region. Its main idea is to distribute the heavy particles in the whole domain and light particles in the concerned local region, such that the computational cost can be reduced without sacrificing its accuracy. The further study will be published later.

References

Antuono, M., Colagrossi, A., Marrone, S. and Molteni, D. (2010), "Free-surface flows solved by means of SPH schemes with numerical diffusive terms", *Computer Physics Communications*, Vol. 181 No. 3, pp. 532-549.

Ataie-Ashtiani, B. and Farhadi, L. (2006), "A stable moving-particle semi-implicit method for free surface flows", *Fluid Dynamics Research*, Vol. 38 No. 4, pp. 241-256.

Chen, X.D., Ma, D.J., Yang, V. and Popinet, S., (2013), "High-fidelity simulations of impinging jet atomization", *Atomization and Sprays*, Vol. 23 No. 12, pp. 1079-1101.

Chihiro I., Watanabe T. and Himeno T., (2008), "Study on atomization process of liquid sheet formed by impinging jets", *44th AIAA/ASME/SAE/ASEE Joint Propulsion Conference & Exhibit, 21-23 July, Hartford, CT*.

Deshpande, S.S. and Trujillo, M.F. (2013), "Distinguishing features of shallow angle plunging jets", *Physics of Fluids*, Vol. 25 No. 8, pp. 082103-1-082103-17.

Deshpande, S.S., Trujillo, M.F., Wu, X.J. and Chahine, G. (2012), "Computational and experimental characterization of a liquid jet plunging into a quiescent pool at shallow inclination", *International Journal of Heat and Fluid Flow*, Vol. 34, pp. 1-14.

Khayyer, A. and Gotoh, H. (2008), "Development of CMPS method for accurate water-surface tracking in breaking waves", *Coastal Engineering Journal*, Vol. 50 No. 2, pp. 179-207.

Khayyer, A. and Gotoh, H. (2010), "A higher order Laplacian model for enhancement and stabilization of pressure calculation by the MPS method", *Applied Ocean Research*, Vol. 32 No. 1, pp. 124-131.

Khayyer, A. and Gotoh, H. (2012), "A 3D higher order Laplacian model for enhancement and stabilization of pressure calculation in 3D MPS-based simulations", *Applied Ocean Research*, Vol. 37, pp. 120-126.

Khayyer, A., Gotoh, H. and Shao, S.D. (2009), "Enhanced predictions of wave impact pressure by improved incompressible SPH methods", *Applied Ocean Research*, Vol. 31 No. 2, pp. 111-131.

Koshizuka, S. and Oka, Y. (1996), "Moving-particle semi-implicit method for fragmentation of incompressible fluid", *Nuclear Science and Engineering*, Vol. 123 No. 3, pp. 421-434.

Koshizuka, S., Nobe, A. and Oka, Y. (1998), "Numerical analysis of breaking waves using the moving particle semi-implicit method", *International Journal for Numerical Methods in Fluids*, Vol. 26 No. 7 pp. 751-769.

Lee, B.H., Park, J.C. and Kim, M.H. (2011), "Step-by-step improvement of MPS method in simulating violent free-surface motions and impact-loads", *Computer Methods in Applied Mechanics and Engineering*, Vol. 200 Nos 9-12, pp. 1113-1125.

Ma, Q.W. (2008), "A new meshless interpolation scheme for MLPG_R method", *Computer Modeling in Engineering & Sciences*, Vol. 23 No. 2, pp. 75-89.

Michell, J.H. (1890), "On the theory of free stream lines", *Philosophical Transactions of the Royal Society of London*, Vol. 181, pp. 389-431.

Milne-Thomson, L.M. (1962), *Theoretical hydrodynamics*, 4th ed., Macmillan & Co. Ltd, London.

Pan, X.J. and Zhang, H.X. (2008), "A study on the oscillations appearing in pressure calculation for sloshing simulation by using moving-particle semi-implicit method", *Chinese Journal of Hydrodynamics*, Vol. 23 No. 4, pp. 453-463.

Qiang, H.F., Han, Y.W., Wang, G. and Liu, H. (2013), "Numerical analysis of atomization process of liquid with power law model based on SPH method", *Journal of Propulsion Technology*, Vol. 34 No. 2, pp. 240-247.

Reichl, P.J., Morris, P., Hourigan, K., Thompson, M.C. and Stoneman, S.A.T. (1998), "Smooth particle hydrodynamics simulation of surface coating", *Applied Mathematical Modelling*, Vol. 22 No. 12, pp. 1037-1046.

Shakibaeinia, A. and Jin, Y.C. (2012), "MPS mesh-free particle method for multiphase flows", *Computer Methods in Applied Mechanics and Engineering*, Vols 229-232, pp. 13-26.

Shibata, K., Koshizuka, S. and Sakai, M., (2012), "Lagrangian simulations of ship-wave interactions in rough seas", *Ocean Engineering*, Vol. 42, pp. 13-25.

Sriram, V. and Ma, Q.W. (2012), "Improved MLPG_R method for simulating 2D interaction between violent waves and elastic structures", *Journal of Computational Physics*, Vol. 231 No. 22, pp. 7650-7670.

Tanaka, M. and Masunaga, T. (2010), "Stabilization and smoothing of pressure in MPS method by Quasi-compressibility", *Journal of Computational Physics*, Vol. 229 No. 11, pp. 4279-4290.

Tang, Z.Y., Zhang, Y.X., Li, H.Z. and Wan D.C. (2014), "Overlapping MPS method for 2D free surface flows", *Proceedings of the 24th International Ocean and Polar Engineering Conference*, *Busan*, pp. 411-419.

Touzé, D.L., Barcarolo, D.A., Kerhuel, M., Leboeuf, F., Caro, J., Quinlan, N., Lobovsky, L., Basa, M., Colagross, A., Marrone, S., Marongiu, J.-C., Leffe, M. de and Guilcher, P.-M. (2012), "Investigation of SPH variants for violent flows simulations within the NextMuSE initiative", *2nd International Conference on Violent Flows*, *Nantes*, pp. 246-252.

Zhang, C., Zhang, Y.X., and Wan, D.C. (2011), "Comparative study of SPH and MPS methods for numerical simulations of dam breaking problems", *Chinese Journal of Hydrodynamics*, Vol. 26 No. 6, pp. 736-746.

Zhang, Y.X. and Wan, D.C. (2011a), "Application of MPS in 3D dam breaking flows", *Scientia Sinica Phys, Mech & Astron*, Vol. 41 No. 2, pp. 140-154.

Zhang, Y.X. and Wan D.C. (2011b), "Apply MPS method to simulate motion of floating body interacting with solitary wave", *Proceedings of the 7th International Workshop on Ship Hydrodynamics*, *16-19 September*, *Shanghai*.

Zhang, Y.X. and Wan D.C. (2012), "Numerical simulation of liquid sloshing in low-filling tank by MPS", *Journal of Hydrodynamics*, Vol. 27 No. 1, pp. 100-107.

Zhang, Y.X. and Wan, D.C. (2014), "Comparative study of MPS method and level-set method for sloshing flows", *Journal of Hydrodynamics*, Vol. 26 No. 4, pp. 577-585.

Zhang, Y.X., Tang, Z.Y. and Wan, D.C. (2013), "Numerical simulation of green water incidents based on parallel MPS method", *Proceedings of the 23rd International Offshore and Polar Engineering Conference*, *Anchorage, AK*, pp. 931-938.

Zhang, Y.X., Yang, Y.Q., Tang, Z.Y. and Wan, D.C. (2014), "Parallel MPS method for three-dimensional liquid sloshing", *Proceedings of the 24th International Ocean and Polar Engineering Conference*, *Busan*, pp. 257-264.

Corresponding author
Professor Decheng Wan can be contacted at: dcwan@sjtu.edu.cn